Title
Large-Scale Combination Direct Shear/Simple Shear Device for Tire-Derived Aggregate

Journal
Geotechnical Testing Journal, 41(2)

ISSN
0149-6115

Authors
Fox, Patrick J
Thielmann, Stuart S
Sanders, Michael J
et al.

Publication Date
2018-03-01

DOI
10.1520/gtj20160245

Peer reviewed

FINAL manuscript submitted to the ASTM *Geotechnical Testing Journal* June 2017

Large-Scale Combination Direct Shear/Simple Shear Device for Tire-Derived Aggregate

Patrick J. Fox Ph.D., P.E., Shaw Professor and Head, Dept. of Civil and Environmental Engineering, The Pennsylvania State University, 212 Sackett, University Park, Pa 16802-1408; pjfox@engr.psu.edu

Stuart S. Thielmann, M.S., Geotechnical Engineer, GeoEngineers, Inc., 1101 Fawcett Ave., Suite 200, Tacoma, WA 98402; sthielmann@geoengineers.com

Michael J. Sanders, M.S., Development Engineer, Dept. of Structural Engineering, University of California - San Diego, 9500 Gilman Dr., La Jolla, CA 92093-0085; mjsander@ucsd.edu

Christopher Latham, Ph.D. Product Development Engineer, Dept. of Structural Engineering, University of California - San Diego, 9500 Gilman Dr., La Jolla, CA 92093-0085; clatham@ucsd.edu

Ismaail Ghaaowd, M.S., Doctoral Candidate, Dept. of Structural Engineering, University of California - San Diego, 9500 Gilman Dr., La Jolla, CA 92093-0085; ighaaowd@ucsd.edu

John S. McCartney, Ph.D., P.E., Associate Professor, Dept. of Structural Engineering, University of California - San Diego, 9500 Gilman Dr., La Jolla, CA 92093-0085; mccartney@ucsd.edu

ABSTRACT: This paper describes a novel large-scale device capable of performing both direct shear and simple shear tests to evaluate shear deformation and strength properties of Type B tire-derived aggregate (TDA). The device consists of stacked tubular steel members that can be locked as upper and lower rigid sections to displace relative to one another in direct shear or pinned at the ends to translate in simple shear. For both configurations, the TDA specimen has a length of 3048 mm, a width of 1220 mm, and an initial height up to 1830 mm. The upper rigid section of the device can also be used to conduct interface direct shear tests. Vertical stress is applied to the top surface of the specimen using dead weights and horizontal shearing force is applied using two hydraulic actuators in displacement-control mode. Typical results from internal direct shear, concrete interface direct shear, and cyclic simple shear tests are presented. In direct shear mode, the device allows for mobilization of peak shear strength and, in simple shear mode, for evaluation of shear stiffness and damping ratio under large strain conditions for TDA with large particle size.

KEYWORDS: Large-scale testing, direct shear, interface direct shear, simple shear, tire-derived aggregate

RUNNING TITLE: Large Combination Direct Shear/Simple Shear Device

INTRODUCTION

Approximately 270 to 290 million light duty and commercial tires are discarded each year in the United States (RMA 2011, 2014). A significant percentage of these waste tires historically have been disposed in landfills, where they take up valuable space, or stockpiled in often unsightly and unsanitary surface impoundments. Tires also are potentially combustible and have characteristics that make disposal difficult. As a result, there is a strong need for recycling and beneficial reuse of waste tires, and civil engineering construction constitutes one of the major markets for these efforts (Geosyntec 2008; RMA 2011).

Waste tires can be recycled to produce tire-derived aggregate (TDA) for construction. TDA consists of a blend of tire chips (2 to 50 mm) and tire shreds (50 to 300 mm), and is more suitable as a construction material when the tire shearing process cleanly cuts the particle edges (Geosyntec 2008). One of the primary benefits of TDA as an alternative to mineral soil aggregate is the low unit weight, which is about one-third to one-half of typical compacted soil. TDA also has other distinctive properties, such as free drainage, high thermal insulation capacity, good vibration damping, and high compressibility. TDA is generally inexpensive compared to other lightweight fill materials and has been used in a wide variety of construction applications, including subgrade, embankment, and trench fills (Geisler et al. 1989; Bosscher et al. 1992; Ahmed and Lovell 1993; Bosscher et al. 1997; Hoppe 1998; Salgado et al. 2003; Yoon et al. 2006; Humphrey 2008; Ahn et al. 2014), backfills for retaining walls and bridge abutments (Reid and Soupir 1998; Tatlisoz et al. 1998; Tweedie et al. 1998a,b; Lee et al. 1999; Humphrey et al. 2000; Humphrey 2008; Xiao et al. 2012; Ahn and Cheng 2014), subgrade thermal insulation (Eaton et al. 1994; Humphrey and Eaton 1995; Benson et al. 1996; Lawrence et al. 1999), drainage layers for highways (Lawrence et al. 1999), vibration damping layers below rail lines

(Wolfe et al. 2004), drainage and daily cover layers for landfills (Edil et al. 1992; Duffy 1996; Jesionek et al. 1998; Reddy and Saichek 1998; Park et al. 2003; Aydilek et al. 2006; Warith and Rao 2006; Reddy et al. 2010), leach fields for septic systems (Envirologic 1990; Spagnoli et al. 2001; Grimes et al. 2003), and protective cushions and seismic isolation layers for earthquake engineering design (Hazarika et al. 2008; Tsang 2008).

TDA can be broadly classified according to predominant particle size into Type A and Type B materials, as summarized in Table 1. Type B TDA includes larger particles and therefore requires less processing and is more cost-effective than Type A TDA for earth fill applications. Larger particles also decrease the amount of exposed steel, which reduces the potential for self-heating reaction (Humphrey 2005). TDA can be mixed with soil prior to construction to improve mechanical properties, such as compressibility and shear strength, and minimize self-heating (Edil and Bosscher 1994; Bernal et al. 1996; Lee et al. 1999; Salgado et al. 2003; Zornberg et al. 2004; Yoon et al. 2006; Tiwari et al. 2012); however, this requires mixing process control on a field scale such that final proportions are within project specifications. The higher unit weight and additional work and cost involved with material preparation is a disincentive for the use of TDA-soil mixtures and, thus, pure Type B TDA is often preferred for fills and embankments. In this case, limits are placed on TDA layer thickness to prevent self-heating (Table 1).

Shear stiffness and strength information are needed for design of many civil engineering applications involving TDA, such as embankments and retaining walls; however, only limited data are available for Type B TDA materials because conventional testing devices cannot accommodate the large particle size. Triaxial tests have been conducted on granulated rubber, small tire chips, and tire chip-soil mixtures with particle sizes of generally 50 mm or less (Bressette 1984; Ahmed 1993; Benda 1995; Masad et al. 1996; Wu et al. 1997; Lee et al. 1999;

Yang et al. 2002) and, although stress-strain and volume change behavior can be evaluated, the size and displacement range of the typical triaxial cell do not allow for Type B TDA material. Direct shear devices generally permit larger shear displacements (e.g., Fox et al. 2006); however, these displacements often are too small to measure peak shear strengths (Humphrey et al. 1993; Foose et al. 1996; Bernal et al. 1997; Tatlisoz et al.1998; Yang et al. 2002; Xiao et al. 2013). As a result, TDA shear strength often is defined at a specified shear displacement, which allows for comparison between tests but may lead to significant variations in reported shear strength parameters. Similarly, dynamic properties (e.g., stiffness and damping) of granulated rubber and rubber-sand mixtures have been reported using a variety of tests, but only for particle sizes smaller than 10 mm (Feng and Sutterer 2000; Kaneko et al. 2003; Pamukcu and Akbulut 2006; Kim and Santamarina 2008; Anastasiadis et al. 2012; Senetakis et al. 2012; Senetakis and Anastasiadis 2015). Measurements of interface shear strength and pullout behavior of TDA with different materials also are relatively scarce (Bernal et al. 1997; Tatlisoz et al. 1998; O'Shaughnessy and Garga 2000). In the absence of adequate data, engineering designs using Type B TDA have been based on conservative parameters, which render the material less competitive as an alternative choice for construction applications.

To address this need, a novel large-scale combination direct shear/simple shear testing device was designed and constructed at the University of California-San Diego. The volume of the test specimen is sufficiently large to accommodate Type B TDA materials. In direct shear mode, the device allows for mobilization of peak shear strength and, in simple shear mode, for evaluation of shear stiffness and damping ratio under large strain conditions. The design of the device is first presented, followed by typical results for internal direct shear, concrete interface direct shear, and cyclic simple shear tests on Type B TDA.

EQUIPMENT DESIGN

Overview

The combination shear device was designed to permit testing of large specimens of Type B TDA materials in both direct shear and simple shear modes. The shear box has interior plan dimensions of 3048 mm (length) × 1220 mm (width) and can accommodate specimens with initial heights up to 1830 mm, which yields an initial specimen volume up to 6.80 m^3. Type B TDA has a predominant particle size range of 150 to 300 mm, and thus the minimum dimension (width) of the specimen is four times larger than the maximum particle size. The sides of the box in the longitudinal direction (i.e., parallel to shear) consist of ten horizontal steel tubular members. At both ends of the box, these tubes are attached to vertical steel end plates using pinned connections. Each end plate consists of upper and lower parts that can be disconnected to displace relative to one another for direct shear or rigidly connected for simple shear. In direct shear mode, the device permits shear displacements up to 715 mm and thus allows for mobilization of peak shear strength for Type B TDA. In simple shear mode, the device permits shear strain amplitudes up to 30% and thus allows for evaluation of shear stiffness and damping ratio under large strain conditions.

The device includes a variety of sensors to record data for direct shear and simple shear tests. Each actuator contains a load cell to measure axial force. Tiltmeters are used to indicate angular displacement of the actuators from horizontal and angular displacement of the end plates from vertical (simple shear mode). A string potentiometer is used to measure horizontal displacement of the device. Displacement transducers are used to measure vertical displacement at each corner of the top section, which indicates specimen volume change and tilting of the top section (direct shear mode).

Direct Shear Configuration

In the direct shear configuration, the device consists of a split box with a top section that travels over a bottom section in the conventional manner, as shown in Figure 1. The longitudinal steel tubes are locked using four diagonal braces (not shown) attached to the outside of the device (i.e., one on each side of both sections), such that the top and bottom sections remain rigid. This forces relative displacement to occur on a horizontal plane through the TDA specimen at the level of the gap between the sections. Vertical stress is applied to the upper surface of the TDA specimen using a rigid top plate and steel/concrete dead weights. Tests with low applied vertical stress are conducted using only the top plate or with dead weights stacked on the top plate, as shown in Fig. 1(a). Tests with high applied vertical stress require additional dead weights that are carried using a "saddle" frame to lower the center of gravity and reduce the potential for tipping instability of the load, as shown in Fig. 1(b). Vertical stresses up to approximately 80 kPa can be applied to a TDA specimen using the saddle frame.

Horizontal shear force is applied by two hydraulic actuators, as shown in Figure 2. The actuators are connected to the top section using slots that permit vertical alignment and positioned at or slightly below the level of the gap to minimize applied moments to the TDA specimen. The actuators can be operated in force-control or displacement-control mode, with displacement control generally preferred to permit measurement of post-peak response. The uppermost steel tube on each side of the bottom section extends out an additional 1180 mm in the direction of shear to provide stability to the top section in the event of tipping. These tube extensions are not contacted during a direct shear test and provide no frictional resistance.

Design details for the longitudinal steel tubes are presented in Figure 3. Each tube has a square cross section (152 mm × 152 mm) and a clear vertical distance of 25.4 mm between the adjacent tubes. This clear distance remains constant for direct shear tests because the top and bottom sections of the device are rigid. For simple shear tests (described below), this clear distance decreases with increasing shear strain of the device. To prevent TDA material from intruding into the clear spaces between the tubes, each tube has a vertical "shingle" welded to the inside face. The shingles are longitudinal plates with a thickness of 6.4 mm and a tapered leading edge, which span the clear space and do not contact the adjacent tube (gap = 3.2 mm) to minimize friction during simple shear tests.

The top and bottom surfaces of the device are fitted with transverse ribs, shown for the bottom surface in Figure 4(a), to reduce slippage of the TDA specimen at these boundaries during shear. The interior walls are lined with thin plastic sheeting to minimize friction and facilitate shear-induced volume change of the specimen. The plastic sheeting also keeps small debris from filling the 3.2 mm gap between each shingle and the adjacent tube, which would introduce extra friction for simple shear tests. Interface direct shear tests can be conducted when various materials are placed in the bottom section of the device, such as the Portland cement concrete block shown in Figure 4(b). In this case, the top section is filled with TDA material and then pulled over the bottom section to measure interface shear strength in the conventional manner. In direct shear mode, the device operates without frictional resistance because shear force is measured at the hydraulic actuators and the top section displaces over the TDA or interface material in the bottom section with no device (i.e., metal-on-metal) contact.

Simple Shear Configuration

In the simple shear configuration, the four diagonal cross-braces are removed and the upper and lower parts of the vertical steel plates at each end of the shear box are rigidly connected using steel bars attached to the outside. This permits the box to deform as a parallelogram when shear force is applied to one end using the hydraulic actuators, as shown in Figure 5(a). The actuator stroke produces back-and-forth cyclic shear strain γ (= dx/H), where dx is the horizontal displacement measured using a string potentiometer at elevation H = 1600 mm. The maximum shear strain amplitude for the device is ±30%. Figure 5(b) shows a photograph of a simple shear test with low applied vertical stress (i.e., no saddle). In simple shear mode, the device operates nearly without frictional resistance because shear forces are measured at the hydraulic actuators, the shingles do not contact adjacent steel tubes, and the steel tubes are connected to the vertical end plates using pinned connections.

MATERIAL

Tests were performed using a single batch of Type B TDA material obtained from the California Department of Resources Recycling and Recovery (CalRecycle). The material had a specific gravity of 1.15, which is consistent with the typical range of 1.02 to 1.27 for TDA (Bressette 1984; Humphrey et al. 1992; Humphrey and Manion 1992; Ahmed 1993). Particle size data, as obtained by manual sorting according to maximum particle dimension (i.e., length) and based on dry weight, are presented in Table 2. Particles ranged from 30 to 320 mm in length and 6 to 20 mm in thickness. The median particle size D_{50} = 120 mm. The coefficient of uniformity $C_z = D_{60}/D_{10}$ = 2.21 and the coefficient of curvature $C_c = (D_{30})^2/(D_{60}\ D_{10})$ = 1.02, which suggests that this TDA material is poorly graded using specifications for natural gravels (ASTM D2487).

PROCEDURES

Specimen Preparation

Preparation procedures for the TDA specimens were similar for both direct shear and simple shear tests. The TDA material was tested in the air-dry condition and stored in large bags, each of which was numbered and had a measured total weight of approximately 3 kN. Before placement of TDA into the device, the interior walls were lined with two layers of thin plastic sheeting and depth markers were painted on the plastic to guide the compaction process. TDA was placed in 100 mm-thick loose lifts, each of which required approximately two bags of material and received six passes of a self-propelled rolling and vibrating compactor (total weight = 14.4 kN). The compactor was lifted into the device using a crane and operated by remote control. During compaction, a temporary geomembrane was placed against the sidewalls to protect the plastic sheeting. Visual observations indicated that the TDA material densified during compaction.

After compaction, the initial specimen height was measured manually at the four corners of the top section, vertical stress was applied using dead weights, and the specimen height was measured again. The applied stress remained on the specimen for static loading period of 12 hours minimum (overnight) to accommodate initial creep settlement and associated TDA densification, such as reported by Wartman et al. (2007), prior to the start of the shearing stage.

Direct Shear

After the static loading period, four hydraulic jacks were used to raise the top section and create a gap (150 to 250 mm) between the top and bottom sections. The gap was smaller than the maximum particle length and needed to avoid metal-on-metal contact between the sections at large displacements. The top section can be raised into this position because vertical stress is applied directly to the TDA specimen (through the top plate) and is facilitated by low friction of the plastic sheeting. The load plate and top section were then rigidly connected such that the entire weight of the top part of the device, including TDA, top section frame, load plate, and any dead weights, was completely supported by the TDA material at the shearing surface. This allows for direct calculation of the total vertical force and eliminates frictional resistance from the device during shear.

Once the top section was in position, the actuators were attached to the vertical end plate of the top section and aligned at the elevation of the gap. A string potentiometer was connected from the concrete reaction block to the end plate to measure horizontal displacement. Four displacement transducers were attached at each corner of the top section to measure vertical displacements. During shear, the tips of these transducers slide on stainless steel plates as shown in Figure 6(a). Two tiltmeters (east/west, north/south) also were attached to the vertical end plate of the top section. Finally, prior to the start of shear, the gap thickness and specimen height were measured again at the four corners and the plastic sheeting at the gap was cut around the periphery of the device.

A direct shear test was conducted on a Type B TDA specimen for an initial normal stress of 76.7 kPa on the failure surface. After compaction and loading, the specimen had an initial unit weight of 8.04 kN/m^3 and an initial void ratio of 0.40. Values of void ratio are calculated from known specimen weight, specimen volume, and specific gravity of solids. Shear displacement was applied at a constant rate of 10 mm/min. During the shearing process, TDA material was left behind at the rear of the device and expanded due to stress relief, and some tilting of the top section was observed at large displacements, as shown in Figure 7(a). Test data are corrected for top section tilt, actuator tilt, and decreasing failure surface area to yield normal stress, shear stress, and volume change of the specimen as a function of shear displacement.

Interface Direct Shear

Procedures for interface direct shear tests are similar to those for internal direct shear tests, with the exception that the bottom boundary of the failure surface is replaced by the specified interface material (e.g., concrete or geosynthetic). An interface direct shear test was conducted using Type B TDA and a solid block of Portland cement concrete for an initial normal stress of 77.0 kPa on the failure surface. After compaction and loading, the specimen had an initial unit weight of 7.38 kN/m^3 and initial void ratio of 0.53. Shear displacement was applied at a constant rate of 10 mm/min. Fig. 7(b) shows slide marks on the top of the concrete block for this test.

Simple Shear

Simple shear tests are conducted with the four diagonal cross-braces removed and the upper and lower parts of each vertical end plate rigidly connected. A multi-stage cyclic simple shear test was performed on a single Type B TDA specimen with constant applied stress. After compaction and loading, the specimen had an initial unit weight of 7.07 kN/m^3 and an initial void ratio of 0.60. Including self-weight of the TDA, the vertical stress at the mid-height of the specimen was 76.6 kPa. The test was operated in displacement-control mode and included five stages of progressively increasing shear strain amplitude (γ_a = 0.1, 0.3, 1, 3, and 10%). Each stage consisted of 20 cycles of back-and-forth shearing using a triangular waveform with constant shear strain amplitude and a constant displacement rate of 24 mm/min. at the string potentiometer (H = 1600 mm). The final stage consisted of 20 cycles at the previous amplitude (3%), followed by 20 cycles at the highest amplitude (10%). Vertical settlement of the top plate was measured throughout the test using displacement transducers at the corners. The test required 15.3 hr. to complete, including the five shearing stages and a static waiting period of 30 min. between each stage. Test data are corrected for top plate tilt, actuator tilt, and actuator height to yield shear stress and volume change of the specimen as a function of shear strain.

RESULTS

Direct Shear

Results for the internal direct shear test on Type B TDA are presented in Figures 8 and 9. Fig. 8(a) shows the constant uncorrected normal stress (76.7 kPa) and the corrected normal stress, which increases nonlinearly with increasing horizontal shear displacement and associated reduction in failure surface area under constant normal force. Uncorrected and corrected values of shear stress are shown in Fig. 8(b). Both relationships indicate progressively decreasing shear stiffness up to peak shear strength. The corrected data yield a peak shear strength of 52 kPa at a horizontal displacement of 460 mm. Corresponding mobilized secant friction angles are shown in Fig. 8(c) and indicate a peak value of 30.2° at 403 mm and post-peak strength reduction with continuing displacement.

Vertical displacements at the four corners of the top section of the device (i.e., NE, NW, SE, and SW) during shear are shown in Figure 9(a). The direction of shearing is toward the south and positive values indicate downward displacement. The individual measurements show progressive downward tilting of the south and west sides of the top section and the average of these four measurements indicates a slight downward displacement during shear. The corresponding average volumetric strain calculated from the average vertical displacement is presented in Fig. 9(b) and shows contraction of the Type B TDA material up to 0.82% at a displacement of 278 mm, followed by expansion to the end of the test.

Concrete Interface Shear

Relationships for uncorrected (77.0 kPa) and corrected normal stress, uncorrected and corrected shear stress, and mobilized secant friction angle for the Type B TDA-concrete interface shear test are presented in Fig. 10. As with Fig. 8(a), the corrected normal stress increases nonlinearly with increasing displacement and associated reduction in failure surface area. The uncorrected shear stress reaches a peak, followed by small post-peak strength reduction, whereas the corrected shear stress continues to increase in response to increasing normal stress with a final value of 39.6 kPa at 715 mm. The mobilized secant friction angle reaches a peak of 22.3° at a displacement of 255 mm and then displays slight post-peak strength reduction to the end of the test with a final value of 21.5°. The peak interface secant friction angle occurs at a smaller displacement and represents a 26% reduction as compared to the peak internal secant friction angle for Type B TDA, and the ratio of peak interface to peak internal secant friction angles is 22.3°/30.2° = 0.74. The peak secant friction angle for the Type B-concrete interface is higher than typical soil-concrete interface friction angles measured for silt (14°), silty sand or clayey sand (17°) and clean sand (17-22°), as reported by NAVFAC (1986).

Vertical displacements at the four courses of the top section are shown in Fig. 11(a), and generally display more consistent behavior than corresponding measurements for the internal shear test (Fig. 9a). The measurements indicate progressive downward tilting of the south end of the top section during shear. The average volumetric strain, shown in Fig. 11(b), indicates continuous contraction for the Type B TDA material with a final value of 4.2%. Volumetric contraction was greater for the interface shear test than for the internal shear test, which is attributed to greater material dilation due to particle interlocking at the failure surface for the internal shear test.

Simple Shear

The multi-stage cyclic simple shear test on Type B TDA yields altogether different results than the direct shear tests. Combined relationships for horizontal displacement, shear force, and specimen volumetric strain for all five stages of the test under a constant vertical stress of 76.6 kPa are presented in Fig. 12. The cyclic displacement time history, shown in Fig. 12(a), indicates good actuator control and consistent maximum displacement values for each test stage. Corresponding shear forces, corrected for actuator tilt and top elevation of the TDA specimen, are shown in Fig. 12(b) and display increasing maximum force values with increasing displacement amplitude, as expected, and also with number of cycles for each stage of loading. Measured shear forces during each loading stage are consistent and indicate good frictional connections between the TDA specimen and the upper and lower shearing surfaces. Data from preliminary tests (not shown) revealed that, without the transverse ribs of Figure 4(a), boundary slippage occurred and produced erroneous shear forces with continued cycling. Corresponding values of volumetric strain are shown in Fig. 12(c) and indicate progressive specimen contraction at all stages of the test, including sharp changes in response to higher shear strain amplitude and also progressive contraction with continued cycling during each stage. The slight increase of shear resistance during each stage, as shown in Fig. 12(b), is attributed to increasing volumetric contraction of the TDA specimen with continued cycling under constant vertical stress and shear strain amplitude.

A combined plot of shear stress versus shear strain relationships for all five stages is presented in Fig. 13(a) and shows hysteretic behavior similar to natural soils. The hysteresis loops indicate energy dissipation for each stage and reduction in stiffness of the Type B TDA material with increasing strain amplitude. Little to no stiffness degradation is observed with continued cycling for each stage. Corresponding values of secant shear modulus were calculated at the points of displacement reversal in the conventional fashion and are shown in Fig. 13(b). Secant shear modulus decreases from 2,386 kPa at γ_a = 0.1% to 403 kPa at γ_a = 10%. Based on data provided by Stokoe et al. (1994) and others, these values are approximately ten times lower than for natural granular soils at similar states of stress and shear strain amplitude. Values of damping ratio D indicate relative levels of energy dissipation and were calculated as:

$$D = \frac{1}{4\pi}\frac{A_L}{A_T} \tag{1}$$

where A_L is the total area within the hysteresis loop for a given stage and A_T is the area within a right triangle going from the origin to the peak of the curve, defined as:

$$A_T = \frac{1}{2}\frac{\left[abs(\tau_{\max}) + abs(\tau_{\min})\right]}{2}\frac{\left[abs(\gamma_{\max}) + abs(\gamma_{\min})\right]}{2} \tag{2}$$

where $\tau_{\max}$ and $\tau_{\min}$ are the maximum and minimum shear stresses at opposite ends of the hysteresis loop, and $\gamma_{\max}$ and $\gamma_{\min}$ are the corresponding maximum and minimum shear strains. Values of damping ratio are shown in Figure 13(c) and range from 18% to 21%, with a minimum at γ_a = 1%. The U-shaped trend differs from typical damping ratios for natural granular soils, which are substantially smaller in magnitude and increase monotonically with increasing shear strain amplitude, but interestingly shows similarity to results reported by Nye and Fox (2007) for a hydrated needle-punched geosynthetic clay liner. Volumetric strains at the end of each stage of cyclic shearing (i.e., 20 cycles) are shown in Figure 13(d) and indicate a strongly contractive trend to a final value of 7.9% at γ_a = 10%.

CONCLUSIONS

The following conclusions are reached as a result of the development of a novel large-scale combination direct shear/simple shear testing device and subsequent internal direct shear, concrete interface direct shear, and cyclic simple shear tests conducted on Type B tire-derived aggregate (TDA):

1. The device consists of stacked tubular steel members that can be locked as upper and lower rigid sections to displace relative to one another in direct shear or pinned at the ends to translate in simple shear. For both configurations, the TDA specimen has a length of 3048 mm, a width of 1220 mm, and an initial height up to 1830 mm. The device can also be used to conduct interface direct shear tests using only the upper rigid section.

2. The internal direct shear test indicated that the device produced a displacement range sufficient to characterize the peak shear strength of Type B TDA material. For an initial normal stress of 76.7 kPa, the measured peak secant friction angle was 30.2° and occurred at a horizontal shear displacement of 403 mm.

3. The interface direct shear test indicated that the device produced a displacement range sufficient to characterize the peak shear strength of the interface between Type B TDA and Portland cement concrete. For an initial normal stress of 77.0 kPa, the measured peak secant

friction angle was 22.3° and occurred at a horizontal shear displacement of 255 mm. A slight post-peak strength reduction was observed for this test.

4. The multi-stage cyclic simple shear test indicated that the device produced a displacement range sufficient to characterize the shear stiffness and damping ratio of Type B TDA material under large strain conditions. For a constant vertical stress of 76.6 kPa at specimen mid-height, the measured secant shear modulus decreased from 2,386 kPa at shear strain amplitude γ_a = 0.1% to 403 kPa at γ_a = 10%. Damping ratios ranged from 18% to 21%, with a minimum at γ_a = 1%. Repeatable hysteresis loops and continuous volumetric contraction were observed for each stage of the test.

5. The Type B TDA material experienced volumetric contraction during shear for all three tests. The multi-stage cyclic simple shear test displayed the most volumetric contraction and the internal direct test displayed the least volumetric contraction.

ACKNOWLEDGMENTS

The authors thank the Powell Labs staff in the Department of Structural Engineering at the University of California-San Diego for assistance with the experimental program. This project was funded by the California Department of Resources Recycling and Recovery (CalRecycle). The assistance and support of Stacey Patenaude and Bob Fujii of CalRecycle and Joaquin Wright of GHD is gratefully acknowledged. The contents of this paper reflect the views of the authors and not necessarily the views of the sponsor.

REFERENCES

Ahmed, I. (1993). *Laboratory Study on Properties of Rubber-Soils*, FHWA/IN/JHRP-93/4, Joint Highway Research Project, Indiana Department of Transportation and Purdue University.

Ahmed, I., and Lovell, C.W. (1993). "Rubber soils as lightweight geomaterials." *Transportation Research Record No. 1422*, Transportation Research Board, Washington, D.C., 61-70.

Ahn, I.-S., and Cheng, L. (2014). "Tire derived aggregate for retaining wall backfill under earthquake loading." *Construction and Building Materials*. Vol. 57, 105-116.

Ahn, I.-S., Cheng, L., Fox, P. J., Wright, J., Patenaude, S., and Fujii, B. (2014). "Material properties of large-size tire derived aggregate for civil engineering applications," *Journal of Materials in Civil Engineering*, DOI: 10.1061/(ASCE)MT.1943-5533.0001225, 11 p.

ASTM D2487 (2011). Standard Practice for Classification of Soils for Engineering Purposes (Unified Soil Classification System). ASTM International, West Conshohocken, PA.

ASTM D6270 (2012). Standard Practice for Use of Scrap Tires in Civil Engineering Applications. ASTM International, West Conshohocken, PA.

Anastasiadis, A., Senetakis, K., Pitilakis, K., Gargala, C., and Karakasi, I. (2012). "Dynamic behavior of sand/rubber mixtures. Part I: Effect of rubber content and duration of confinement on small-strain shear modulus and damping ratio," *Journal of ASTM International*, Vol. 9, No. 2, 19 p.

Aydilek, A. H., Madden, E. T. and Demirkan, M. M. (2006). "Field evaluation of a leachate collection system constructed with scrap tires." *Journal of Geotechnical and Geoenvironmental Engineering*, Vol. 132, No. 8, 990-1000.

Benda, C. C. (1995). "Engineering Properties of Scrap Tires Used in Geotechnical Applications," Report No. 95-1, Vermont Agency of Transportation, Montpelier, VT.

Benson, C. H., Olson, M. A., and Bergstrom, W. R. (1996). "Temperatures of insulated landfill liner." *Transportation Research Record No. 1534*, Transportation Research Board, Washington, D.C., 24-31.

Bernal, A., Lovell, C. W., and Salgado, R. (1996). *Laboratory Study on the Use of Tire Shreds and Rubber-Sand in Backfilled and Reinforced Soil Applications*. FHWA/IN/JHRP-96/12, Joint Highway Research Project, Indiana Department of Transportation and Purdue University, 164 p.

Bernal, A., Salgado, R., Swan, Jr., R. H., and Lovell, C. W. (1997). "Interaction between tire shreds, rubber-sand and geosynthetics." *Geosynthetics International*, Vol. 4, No. 6, 623-643.

Bosscher, P. J., Edil, T. B., and Eldin, N. N. (1992). "Construction and performance of shredded waste-tire test embankment." *Transportation Research Record No. 1345*, Transportation Research Board, Washington, D.C., 44-52.

Bosscher, P. J., Edil, T. B., and Kuraoka, S., (1997). "Design of highway embankments using tire chips." *Journal of Geotechnical and Geoenvironmental Engineering*. Vol. 123, No. 4, 295-304.

Bressette, T. (1984). *Used Tire Material as an Alternative Permeable Aggregate*. FHWA/CL/TL-84/07, Office of Transportation Laboratory, California Dept. of Transportation, Sacramento, CA.

CalRecycle (2016). *Usage Guide: Tire-Derived Aggregate (TDA)*. Publication #DRRR 2016-01545, California Department of Resources Recycling and Recovery, Sacramento, CA.

Duffy, D. P. (1996). "The potential for use of shredded tire chips as a leachate drainage and collection medium: Design, construction and performance considerations," *Proceedings,* *Landfill Design Seminar Using Tire Shreds*, Texas Natural Resource Conservation Commission, Arlington, TX, 115-132.

Eaton, R. A., Roberts, R. J., and Humphrey, D. N. (1994). *Gravel Road Test Sections Insulated with Scrap Tire Chips: Construction and First Year's Results.* Special Report No. 94-21, U.S. Amry Corps of Engineers, Cold Regions Research & Engineering Laboratory, Hanover, NH, 43 p.

Edil, T. B., Fox, P. J., and Ahl, S. W. (1992). "Hydraulic conductivity and compressibility of waste tire chips," *15th Madison Waste Conference*, Madison, Wisconsin, 49-61.

Edil, T. B. and Bosscher, P. J. (1994). "Engineering properties of tire chips and soil mixtures." *Geotechnical Testing Journal*, Vol. 17, No. 4, 453-464.

Envirologic, Inc. (1990). *A Report on the Use of Shredded Scrap Tires in On-site Sewage Disposal Systems*. The Department of Environmental Conservation, State of Vermont, 88 p.

Feng, Z.-Y. and Sutterer, K. G. (2000). "Dynamic properties of granulated rubber/sand mixtures." *Geotechnical Testing Journal*. Vol. 23, No. 3, 338-344.

Foose, G. J., Benson, C. H., and Bosscher, P. J. (1996). "Sand reinforced with shredded waste tires." *Journal of Geotechnical Engineering*. Vol. 122, No. 9, 760-767.

Fox, P. J., Nye, C. J., Morrison, T. C., Hunter, J. G., and Olsta, J. T. (2006). "Large dynamic direct shear machine for geosynthetic clay liners." *Geotechnical Testing Journal*, Vol. 29, No. 5, 392-400.

Geisler, E., Cody, W. K., and Niemi, M. K. (1989). "Tires for subgrade support." *Proceedings, 12th Annual Meeting of the Council on Forest Engineering*, Coeur d'Alene, ID. 56-60.

Geosyntec. (2008). *Guidance Manual for Engineering Uses of Scrap Tires*. Prepared for Maryland Department of the Environment, Project No. ME0012-11, Geosyntec Consultants, Columbia, Maryland.

Grimes, B. H., Steinbeck, S., and Amoozegar, A. (2003). "Analysis of tire chips as a substitute for stone aggregate in nitrification trenches of onsite septic systems: Status and notes on the comparative macrobiology of tire chip versus stone aggregate trenches," *Small Flows Quarterly*, Vol. 4, No. 4, 18-23.

Hazarika, H., Kohama, E., and Sugano, T. (2008). "Underwater shake table tests on waterfront structures protected with tire chips cushion." *Journal of Geotechnical and Geoenvironmental Engineering*, Vol. 134, No. 12, 1706-1719.

Hoppe, E. J. (1998). "Field study of shredded-tire embankment," *Transportation Research Record No. 1619*, Transportation Research Board, Washington, D.C., 47-54.

Humphrey, D. N. (2005). "Tire derived aggregate - A new road building material," *Proceedings, 7th International Conference on the Bearing Capacity of Roads, Railways and Airfields*, Trondheim, Norway, 27-29 June, 6 pp. [CDROM]

Humphrey, D. N. (2008). "Tire derived aggregate as lightweight fill for embankments and retaining walls." *Scrap Tire Derived Geomaterials—Opportunities and Challenges*, H. Hazarika and K. Yasuhara, eds., Taylor & Francis Group, London, 59-81.

Humphrey, D. N., and Eaton, R. A. (1995). "Field performance of tire chips as subgrade insulation for rural roads." *Proceedings, 6th International Conference on Low-Volume Roads*, Transportation Research Board, Washington, D.C., 77-86.

Humphrey, D. N., Sandford, T. C., Cribbs, M. M., Gharegrat, H., and Manion, W. P. (1992). *Tire Chips as Lightweight Backfill for Retaining Walls - Phase I*. A Study for the New England

Transportation Consortium, Department of Civil Engineering, University of Maine, Orono, ME, 137 pp.

Humphrey, D. N. and Manion, W. P. (1992). "Properties of tire chips for lightweight fill." *Proceedings, Conference on Grouting, Soil Improvement, and Geosynthetics*, ASCE, New Orleans, Louisiana, Vol. 2, 1344-1355.

Humphrey, D. N., Sandford, T. C., Cribbs, M. M., and Manion, W. P. (1993). "Shear strength and compressibility of tire chips for use as retaining wall backfill." *Transportation Research Record No. 1422*, Transportation Research Board, Washington, D.C., 29–35.

Humphrey, D. N., Whetten, N., Weaver, J., and Recker, K. (2000). "Tire shreds as lightweight fill for construction on weak marine clay," *Proceedings, International Symposium on Coastal Geotechnical Engineering in Practice*, Balkema, Rotterdam, 611-616.

Jesionek, K. S., Humphrey, D. N., and Dunn, R. J. (1998). "Overview of shredded tire applications in landfills," *Proceedings, Tire Industry Conference*, Clemson University, Clemson, SC, 12 pp.

Kaneko, T., Orense, R. P., Hyodo, M., and Yoshimoto, N. (2003). "Seismic response characteristics of saturated sand deposits mixed with tire chips." *Journal of Geotechnical and Geoenvironmental Engineering*. Vol. 139, No. 4, 633-643.

Lee, J. H., Salgado, R., Bernal, A., and Lovell, C. W. (1999). "Shredded tires and rubber-sand as lightweight backfill." *Journal of Geotechnical and Geoenvironmental Engineering*, Vol. 125, No. 2, 132-141.

Kim, H.-K., and Santamarina, J. C. (2008). "Sand-rubber mixtures (large rubber chips)," *Canadian Geotechnical Journal*, Vol. 45, No. 10, 1457-1466.

Lawrence, B., Humphrey, D., and Chen, L.-H. (1999). "Field trial of tire shreds as insulation for paved roads." *Proceedings, 10th International Conference on Cold Regions Engineering: Putting Research into Practice*, ASCE, Reston, VA, 428-439.

Lee, J. H., Salgado, R., Bernal, A., and Lovell, C. W. (1999). "Shredded tires and rubber-sand as lightweight backfill." *Journal of Geotechnical and Geoenvironmental Engineering*, Vol. 125 No. 2, 132–141.

Masad, E., Taha, R., Ho, C., and Papagiannakis, T. (1996). "Engineering properties of tire/soil mixtures as a lightweight fill material," *Geotechnical Testing Journal*, Vol. 19, No. 3, 297-304.

NAVFAC (1986). *Foundations & Earth Structures*, Design Manual 7.02, Naval Facilities Engineering Command, Alexandria, Virginia, 256 pp.

Nye, C. J., and Fox, P. J. (2007). "Dynamic shear behavior of a needle-punched geosynthetic clay liner." *Journal of Geotechnical and Geoenvironmental Engineering*, Vol. 133, No. 8, 973-983.

O'Shaughnessy, V., and Garga, V. K. (2000). "Tire-reinforced earthfill. Part 2: Pull-out behaviour and reinforced slope design," *Canadian Geotechnical Journal*, Vol. 37, No. 1, 97-116.

Pamukcu, S., and Akbulut, S. (2006). "Thermoelastic enhancement of damping of sand using synthetic ground rubber." *Journal of Geotechnical and Geoenvironmental Engineering*, Vol. 132, No. 4, 501-510.

Park, J. K., Edil, T. B., Kim, J. Y., Huh, M., Lee, S. H., and Lee, J. J. (2003). "Suitability of shredded tyres as a substitute for a landfill leachate collection medium," *Waste Management and Research*, Vol. 21, No. 3, 278-289.

Reddy, K. R., and Saichek, R. E. (1998). "Assessment of damage to geomembrane liners by shredded scrap tires." *Geotechnical Testing Journal*, Vol. 21, No. 4, 307-316.

Reddy, K. R., Stark, T. D., and Marella, A. (2010). "Beneficial use of shredded tires as drainage material in cover systems for abandoned landfills." *Practice Periodical of Hazardous, Toxic, and Radioactive Waste Management*, Vol. 14, No. 1, 47-60.

Reid, R. A., and Soupir, S. P. (1998). "Mitigation of void development under bridge approach slabs using rubber tire chips." *Proc., Conf. on Recycled Materials in Geotechnical Applications*, ASCE, Arlington, VA, 37–50.

RMA (2011). *U.S. Scrap Tire Management Summary 2005-2009*, Rubber Manufacturers Association, Inc., October, Washington, D.C.

RMA (2014). 2013 *U.S. Scrap Tire Management Summary*, Rubber Manufacturers Association, Inc., October, Washington, D.C.

Salgado, R., Yoon, S., and Siddiki, N. Z. (2003). *Construction of Tire Shreds Test Embankment*. FHWA/IN/JTRP-2002/35. Joint Transportation Research Program, Indiana Department of Transportation and Purdue University, 50 p.

Senetakis, K., Anastasiadis, A., Pitilakis, K., and Souli, A. (2012). "Dynamic behavior of sand/rubber mixtures. Part II: Effect of rubber content on G/G_o-γ-DT curves and volumetric threshold strain," *Journal of ASTM International*, Vol. 9, No. 2, 12 p.

Senetakis, K., and Anastasiadis, A. (2015). "Effects of state of test sample, specimen geometry and sample preparation on dynamic properties of rubber-sand mixtures," *Geosynthetics International*, Vol. 22, No. 4, pp. 301-310.

Spagnoli, J., Weber, A. S., and Zicari, L. P. (2001). *The Use of Tire Chips in Septic System Leachfields*. Center for Integrated Waste Management, University of Buffalo, Buffalo, New York, 92 pp.

Stokoe, K. H., II, Hwang, S. K., Lee, J. N.-K., and Andrus, R. D. (1994). "Effects of various parameters on the stiffness and damping of soils at small to medium strains." *Proceedings, 1st International Symposium on Pre-failure Deformation Characteristics of Geomaterials*. Sapporo, Japan, Vol. 2, 785-816.

Tatlisoz, N., Edil, T. B., and Benson, C. H. (1998). "Interaction between reinforcing geosynthetics and soil-tire chip mixtures." *Journal of Geotechnical and Geoenvironmental Engineering*, Vol. 124, No. 11, 1109–1119.

Tiwari, B., Ajmera, B., Moubayed, S., Lemmon, A., and Styler, K. (2012). "Soil modification with shredded rubber tires," *Proceedings, GeoCongress 2012: State of the Art and Practice in Geotechnical Engineering*, ASCE, 3701-3708.

Tsang, H.-H. (2008). "Seismic isolation by rubber–soil mixtures for developing countries." *Earthquake Engineering and Structural Dynamics*, Vol. 37, No. 2, 283-303

Tweedie, J. J., Humphrey, D. N., and Sandford, T. C. (1998a). "Full-scale field trials of tire shreds as lightweight retaining wall backfill under at-rest conditions." *Transportation Research Record No. 1619*, Transportation Research Board, Washington, D.C., 64-71.

Tweedie, J. J., Humphrey, D. N., and Sandford, T. C. (1998b). "Tire shreds as lightweight retaining wall backfill: Active conditions." *Journal of Geotechnical and Geoenvironmental Engineering*, Vol. 124, No. 11, 1061-1070.

Warith, M. A., and Rao, S. M. (2006). "Predicting the compressibility behaviour of tire shred samples for landfill applications." *Waste Management*, Vol. 26, No. 3, 268-276.

Wartman, J., Natale, M. F., and Strenk, P. M. (2007). "Immediate and time-dependent compression of tire derived aggregate," *Journal of Geotechnical and Geoenvironmental Engineering*, Vol. 33, No. 3, 245-256.

Wolfe, S. L., Humphrey, D. N., and Wetzel, E. A. (2004). "Development of tire shred underlayment to reduce groundborne vibration from LRT track." *Proceedings, GeoTrans 2004*, ASCE, Reston, VA, 750-759.

Wu, W. Y., Benda, C. C. and Cauley, R. F. (1997). "Triaxial determination of shear strength of tire chips." *Journal of Geotechnical and Geoenvironmental Engineering*, Vol. 123, No. 5, 479-482.

Xiao, M., Bowen, J., Graham, M., and Larralde, J. (2012). "Comparison of seismic responses of geosynthetically reinforced walls with tire-derived aggregates and granular backfills." *Journal of Materials in Civil Engineering*, Vol. 24, No. 11, 1368-1377.

Xiao, M., Ledezma, M., and Hartman, C. (2013). "Shear resistance of tire-derived aggregate using large-scale direct shear tests." *Journal of Materials in Civil Engineering*, DOI: 10.1061/(ASCE)MT.1943-5533.0001007, 8 p.

Yang, S., Lohnes, R. A., and Kjartanson, B. H. (2002). "Mechanical properties of shredded tires." *Geotechnical Testing Journal*, Vol. 25, No. 1, 44-52.

Yoon, S., Prezzi, M., Siddiki, N. Z., and Kim, B. (2006). "Construction of a test embankment using a sand-tire shred mixture as fill material." *Waste Management*, Vol. 26, No. 9, 1033-1044.

Zornberg, J. G., Cabral, A. R., and Viratjandr, C. (2004). "Behaviour of tire shred-sand mixtures." *Canadian Geotechnical Journal*, Vol. 41, No. 2, 227-241.

TABLE 1: Typical characteristics of TDA materials for field applications (CalRecycle 2016).

Characteristics	**Type A TDA**	**Type B TDA**
Fill class	Class 1	Class 2
Typical size	75-100 mm	150-300 mm
Maximum layer thickness to avoid self-heating reaction*	1 m	3 m
Typical dry unit weight range: (shipping and stockpiling)	3.9-5.5 kN/m^3	3.9-5.5 kN/m^3
Typical dry unit weight range: (compacted)	7.1-8.3 kN/m^3	7.1-7.9 kN/m^3

*ASTM D6270

TABLE 2: Particle size information for Type B TDA material.

Parameter	Value
Particle length	30-320 mm
Particle thickness	6-20 mm
D_{10}	70 mm
D_{50}	120 mm
D_{60}	155 mm
Coefficient of uniformity, C_z	2.21
Coefficient of curvature, C_c	1.02

FIGURE CAPTIONS

FIG. 1: Components of shear device in direct shear mode: (a) Direction parallel to shear; (b) Direction perpendicular to shear with saddle frame (distances in mm).

FIG. 2: Shear device in direct shear mode: (a) Elevation view; (b) Photograph with low applied stress; (c) Photograph with high applied stress.

FIG. 3: Details for longitudinal steel tubes and shingles (distances in mm).

FIG. 4: Boundary conditions: (a) Transverse ribs in bottom section; (b) Portland cement concrete block in bottom section for interface direct shear test.

FIG. 5: Shear device in simple shear mode: (a) Elevation view; (b) Photograph with low applied stress.

FIG. 6: Vertical displacement transducers for measurement of volume change behavior in direct shear mode.

FIG. 7: Direct shear tests: (a) Tilting of top section at large displacements for TDA internal shear test; (b) Slide marks on concrete block for TDA-concrete interface shear test.

FIG. 8: Results for internal direct shear test of Type B TDA: (a) Normal stress; (b) Shear stress; (c) Secant friction angle.

FIG. 9: Results for internal direct shear test of Type B TDA: (b) Vertical displacements; (b) Volumetric strain.

FIG. 10: Results for direct shear test of Type B TDA-concrete interface: (a) Normal stress; (b) Shear stress; (c) Secant friction angle.

FIG. 11: Results for direct shear test of Type B TDA-concrete interface: (a) Vertical displacements; (b) Volumetric strain.

FIG. 12: Results for multi-stage cyclic simple shear test of Type B TDA: (a) Horizontal displacement; (b) Shear force; (c) Volumetric strain.

FIG. 13: Results for multi-stage cyclic simple shear test of Type B TDA: (a) Shear stress versus shear strain; (b) Secant shear modulus; (c) Damping ratio; (d) Volumetric strain.

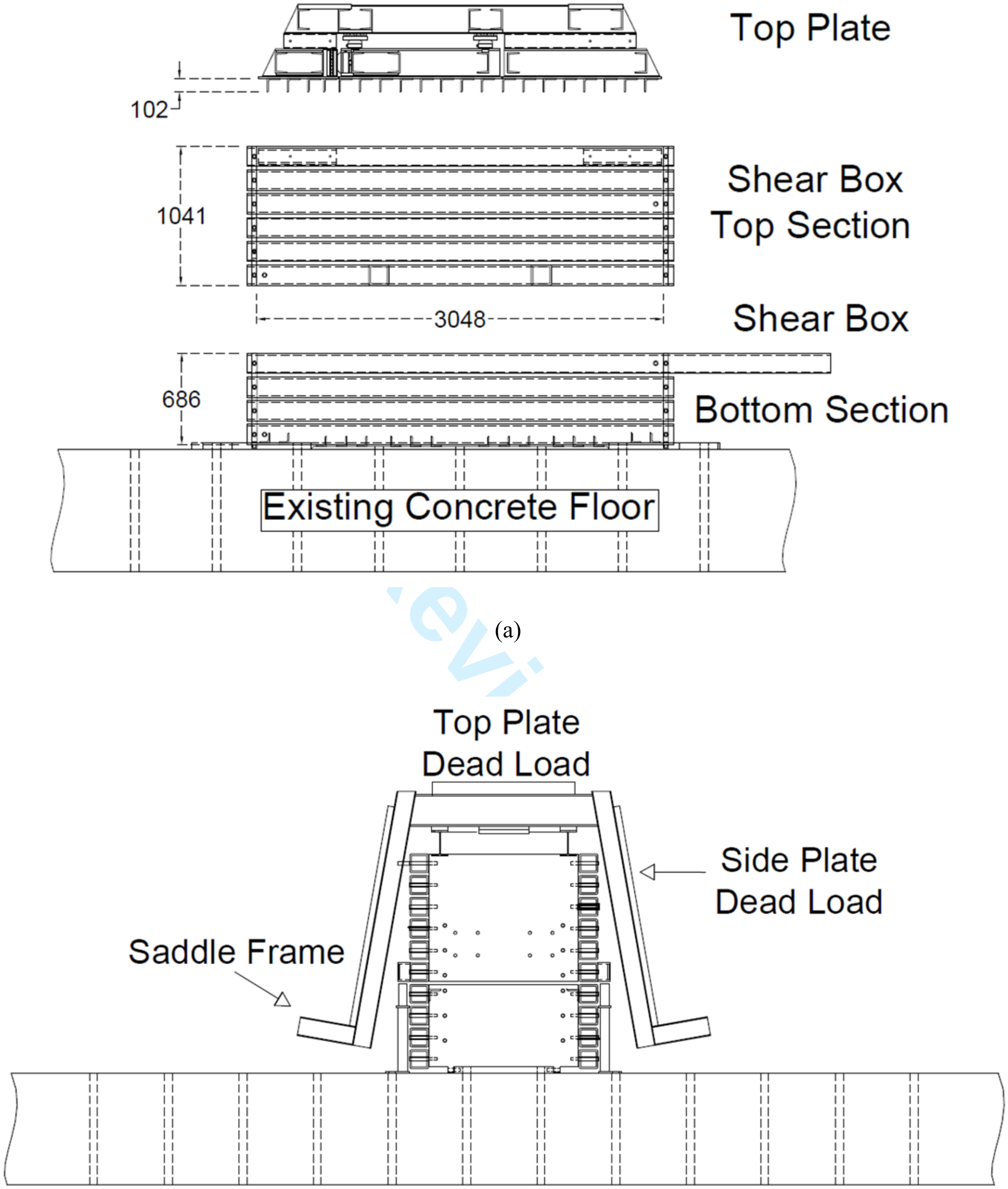
Top Plate
102
1041
Shear Box
Top Section
3048
Shear Box
686
Bottom Section
Existing Concrete Floor
Top Plate
Dead Load
Side Plate
Dead Load
Saddle Frame

(a)

(b)

FIGURE 1

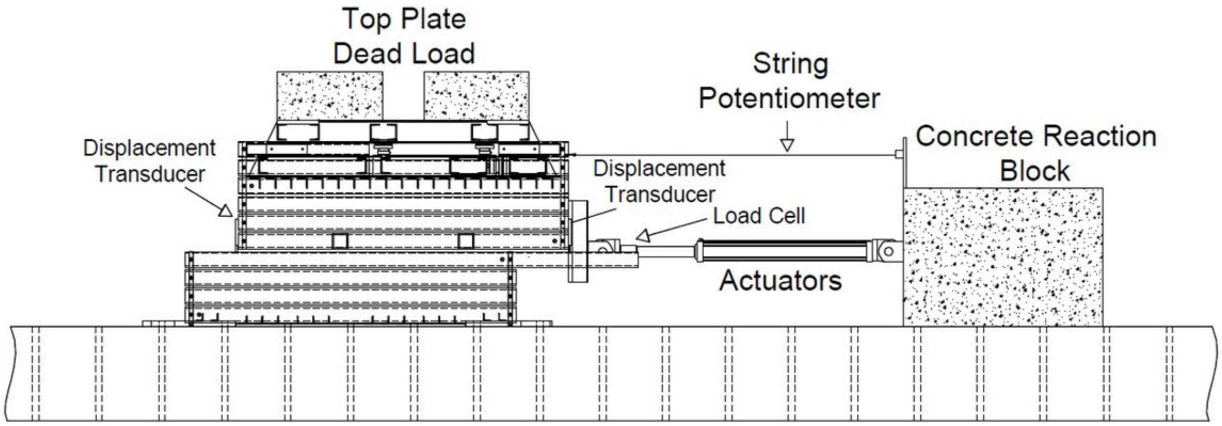
Top Plate
Dead Load
String
Potentiometer
Concrete Reaction
Block
Displacement
Transducer
Displacement
Transducer
Load Cell
Actuators

(a)

(b)

(c)

FIGURE 2

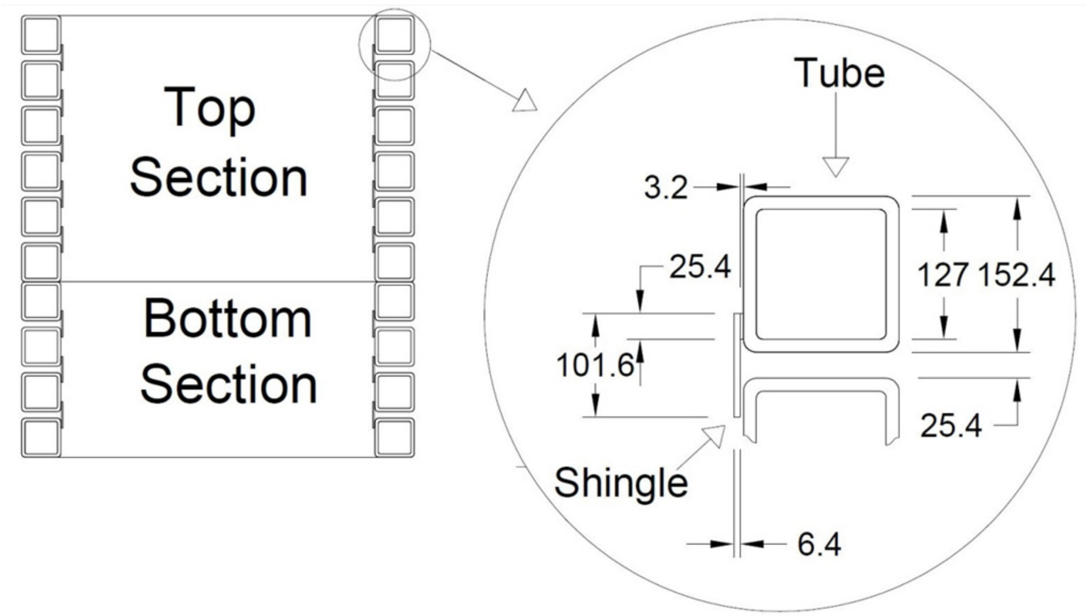
Top
Section
Bottom
Section
Tube
3.2
25.4
101.6
127
152.4
25.4
Shingle
6.4

FIGURE 3

(a)

(b)

FIGURE 4

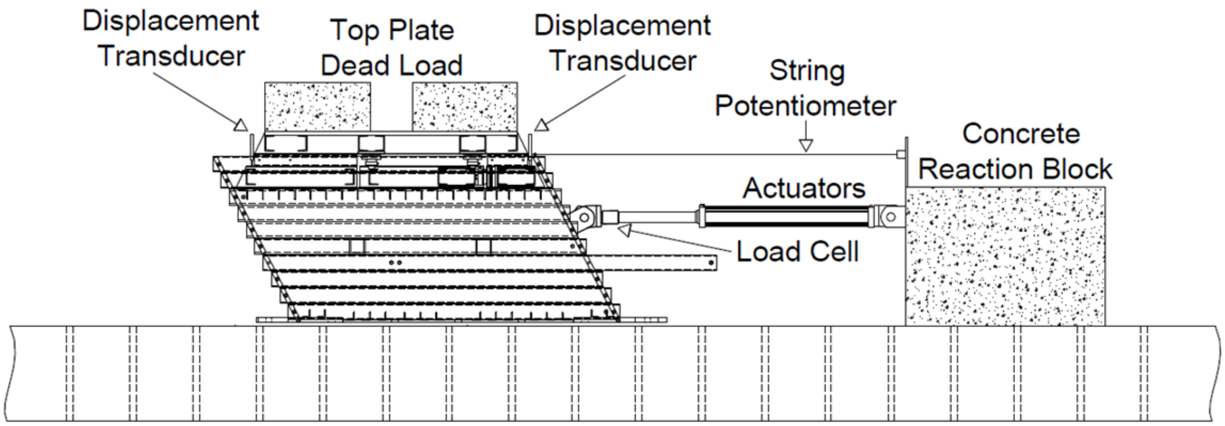
Displacement
Transducer
Top Plate
Dead Load
Displacement
Transducer
String
Potentiometer
Concrete
Reaction Block
Actuators
Load Cell

(a)

(b)

FIGURE 5

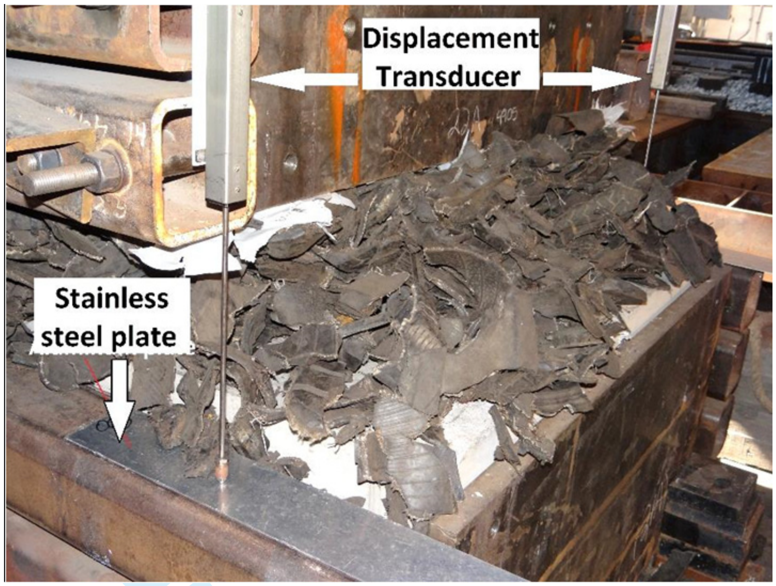

FIGURE 6

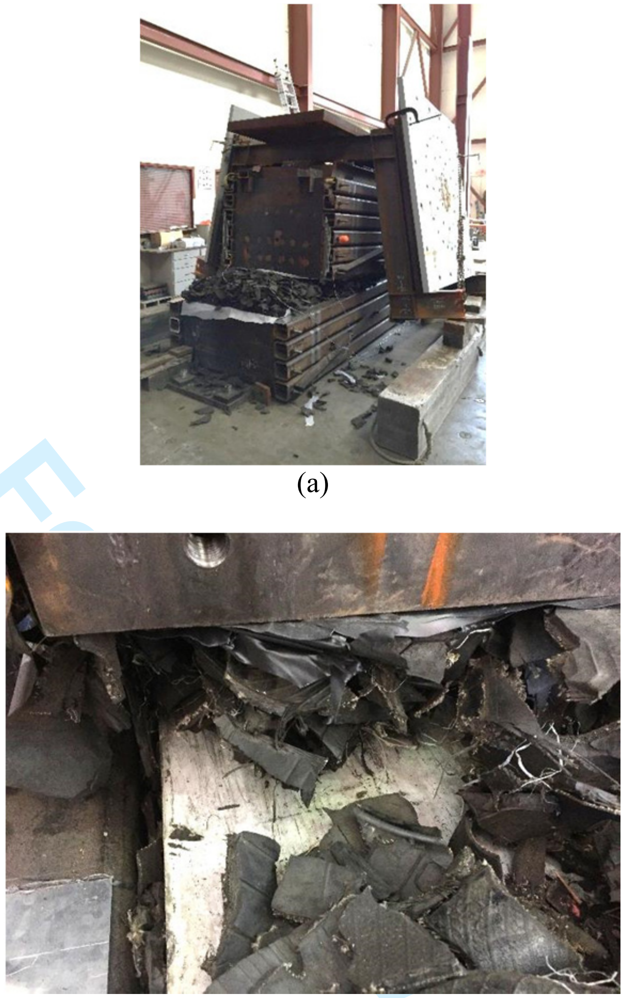

(a)

(b)

FIGURE 7

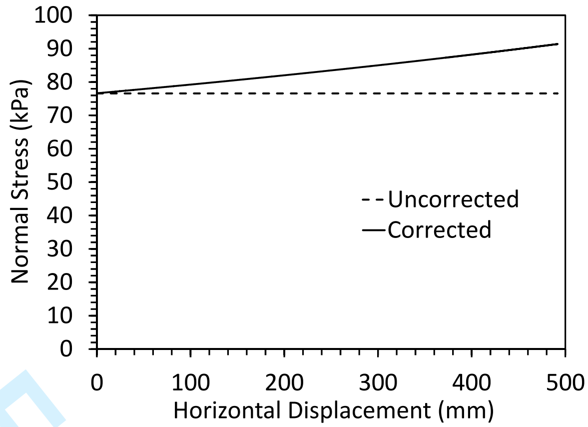
100
90
80
70
60
50
40
30
20
10
0
Normal Stress (kPa)
Uncorrected
Corrected
0
100
200
300
400
500
Horizontal Displacement (mm)

(a)

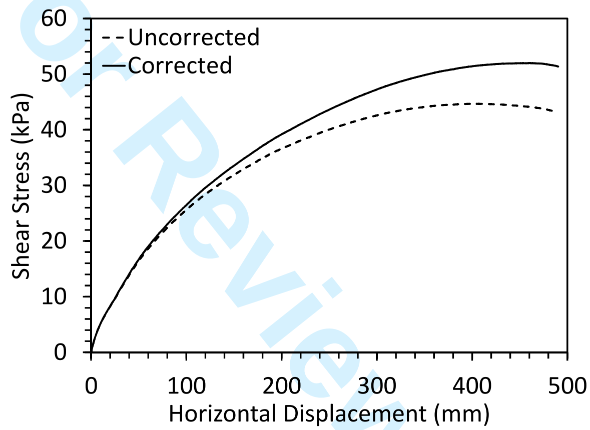
60
50
40
30
20
10
0
Shear Stress (kPa)
Uncorrected
Corrected
0
100
200
300
400
500
Horizontal Displacement (mm)

(b)

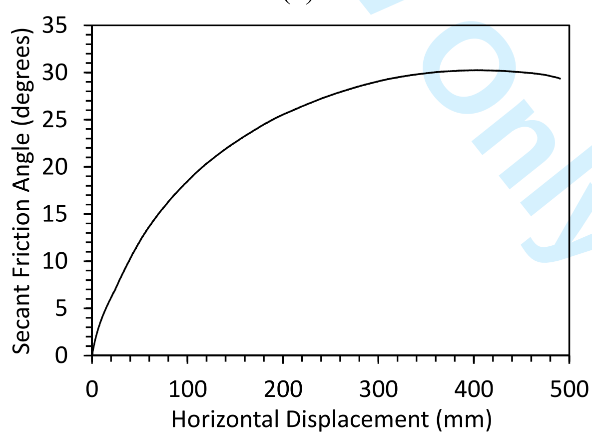
35
30
25
20
15
10
5
0
Secant Friction Angle (degrees)
0
100
200
300
400
500
Horizontal Displacement (mm)

(c)

FIGURE 8

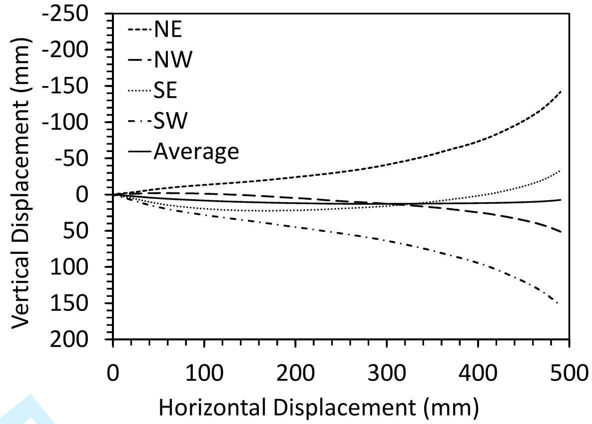
NE
NW
SE
SW
Average
Vertical Displacement (mm)
-250
-200
-150
-100
-50
0
50
100
150
200
0
100
200
300
400
500
Horizontal Displacement (mm)

(a)

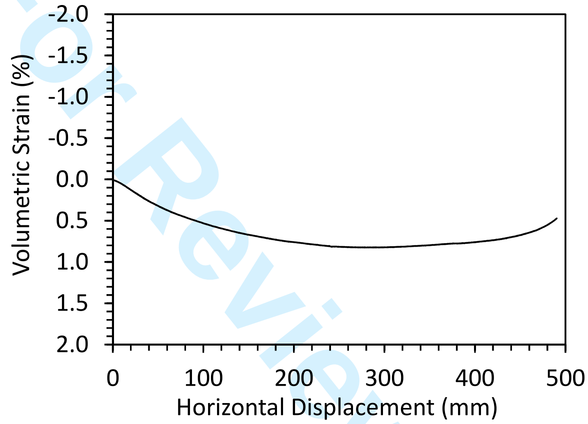
Volumetric Strain (%)
-2.0
-1.5
-1.0
-0.5
0.0
0.5
1.0
1.5
2.0
0
100
200
300
400
500
Horizontal Displacement (mm)

(b)

FIGURE 9

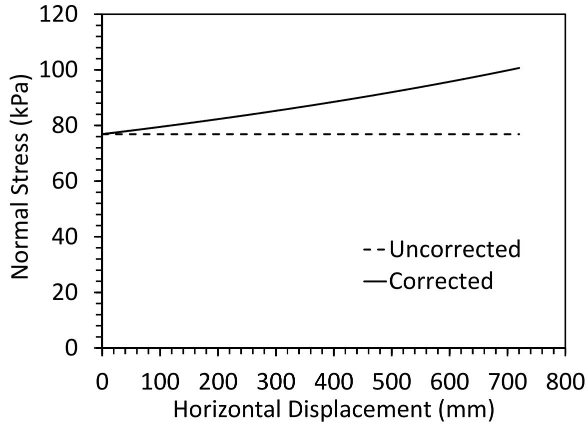

(a)

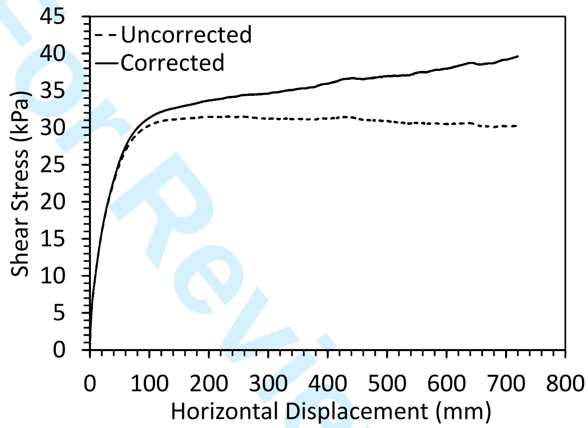

(b)

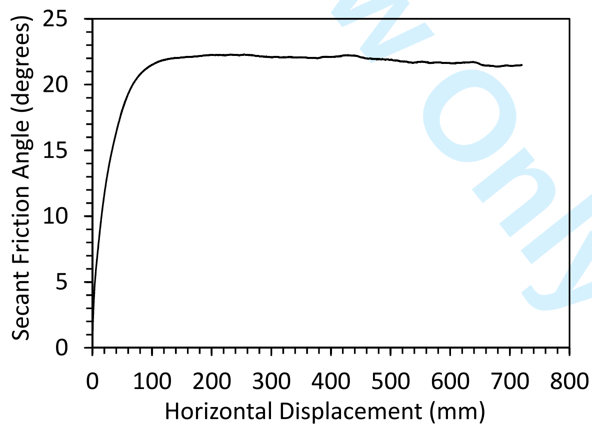

(c)

FIGURE 10

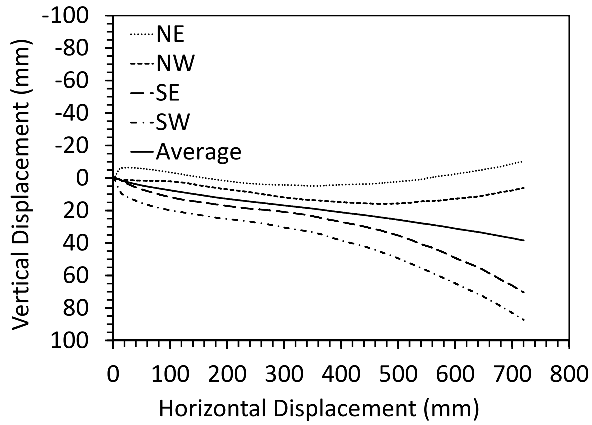
NE
NW
SE
SW
Average
Vertical Displacement (mm)
-100
-80
-60
-40
-20
0
20
40
60
80
100
0 100 200 300 400 500 600 700 800
Horizontal Displacement (mm)

(a)

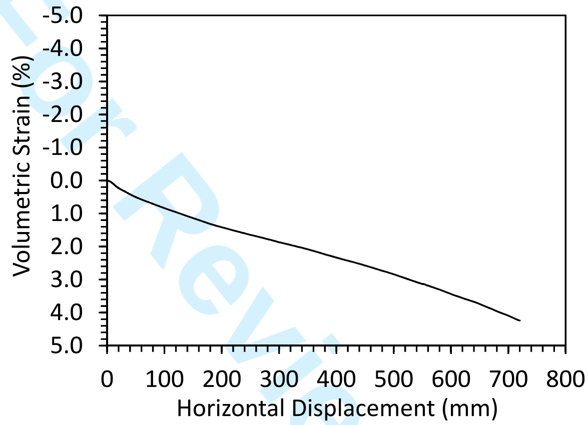
Volumetric Strain (%)
-5.0
-4.0
-3.0
-2.0
-1.0
0.0
1.0
2.0
3.0
4.0
5.0
0 100 200 300 400 500 600 700 800
Horizontal Displacement (mm)

(b)

FIGURE 11

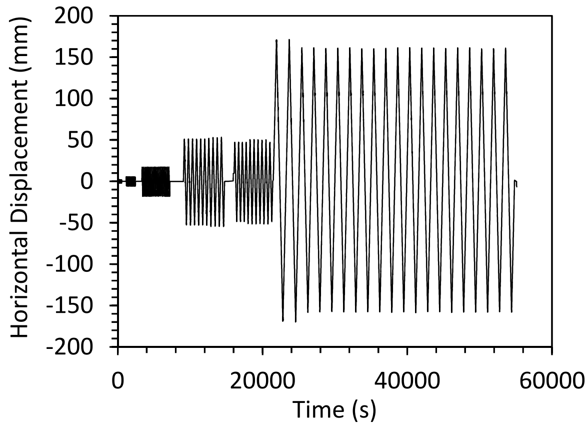

(a)

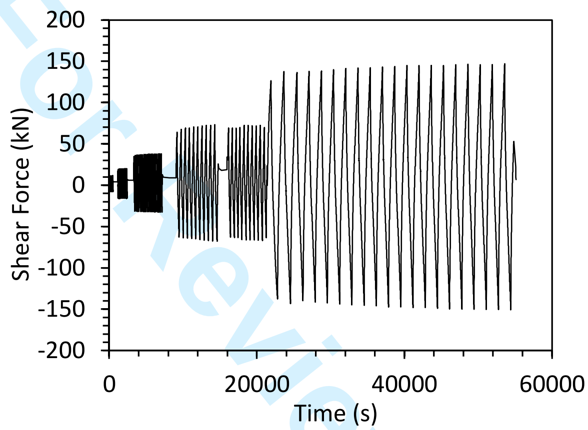

(b)

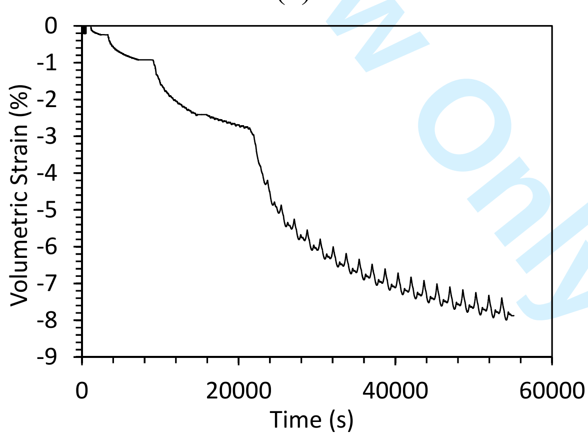

(c)

FIGURE 12

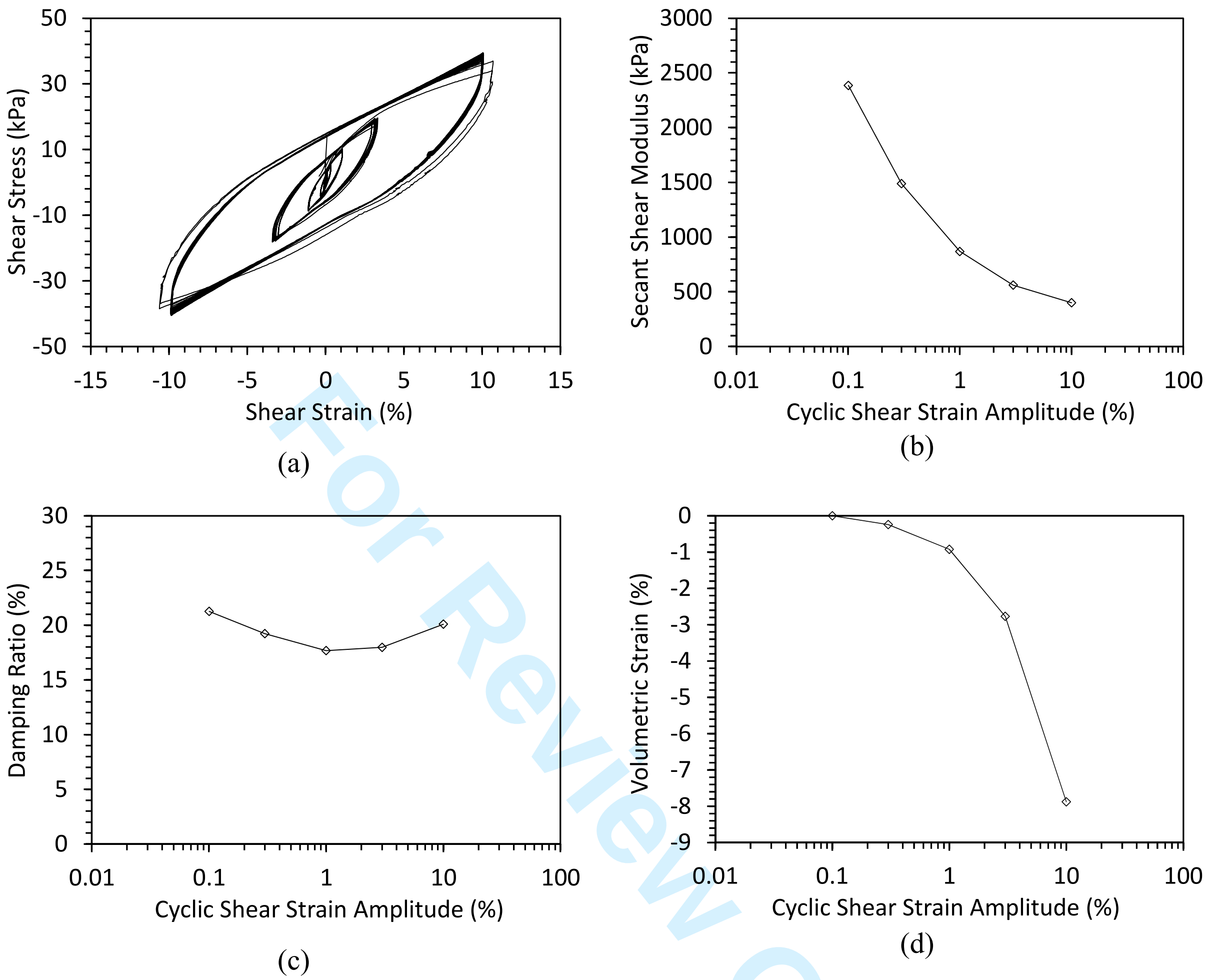
Shear Stress (kPa)
50
30
10
-10
-30
-50
-15
-10
-5
0
5
10
15
Shear Strain (%)
(a)
Secant Shear Modulus (kPa)
3000
2500
2000
1500
1000
500
0
0.01
0.1
1
10
100
Cyclic Shear Strain Amplitude (%)
(b)
Damping Ratio (%)
30
25
20
15
10
5
0
0.01
0.1
1
10
100
Cyclic Shear Strain Amplitude (%)
(c)
Volumetric Strain (%)
0
-1
-2
-3
-4
-5
-6
-7
-8
-9
0.01
0.1
1
10
100
Cyclic Shear Strain Amplitude (%)
(d)

FIGURE 13